

Accretion mediated spin-eccentricity correlations in LISA massive black hole binaries

Mudit Garg,^{1*} Christopher Tiede,² & Daniel J. D’Orazio²

¹*Department of Astrophysics, University of Zurich, Winterthurerstrasse 190, CH-8057 Zürich, Switzerland*

²*Niels Bohr International Academy, Niels Bohr Institute, Blegdamsvej 17, 2100 Copenhagen, Denmark*

Accepted ???, Received ???; in original form ???

ABSTRACT

We examine expected effective spin ($\chi_{\text{eff},1\text{yr}}$) and orbital eccentricity ($e_{1\text{yr}}$) correlations for a population of observable equal-mass massive black hole binaries (MBHBs) with total redshifted mass $M_z \sim [10^{4.5}, 10^{7.5}] M_\odot$ embedded in a circumbinary disc (CBD), one-year before merging in the LISA band. We find a strong correlation between measurable eccentricity and negative effective spin for MBHBs that are carried to merger by retrograde accretion. This is due to the well-established eccentricity pumping of retrograde accretion and the formation of retrograde CBD-aligned mini-discs, as observed in hydrodynamical simulations. Conversely, prograde accretion channels result in positive $\chi_{\text{eff},1\text{yr}}$ and non-measurable $e_{1\text{yr}}$. This clear contrast between the two CBD orientations—and particularly the unique signature of retrograde configurations—provides a promising way to unlock the mysteries of MBHB formation channels in the LISA era.

Key words: accretion, accretion discs – black hole mergers – gravitational waves – quasars:general – methods: numerical

1 INTRODUCTION

Galaxy mergers in the Universe lead to the formation of massive black hole binaries (MBHBs; Begelman et al. 1980). Dynamical friction from stars and gas can bring such MBHBs to parsec scales, but beyond this it becomes inefficient. At these separations, gravitational waves (GWs) alone can not merge the binary within the lifetime of the Universe. This is canonically referred to as the final-parsec problem (Milosavljevic & Merritt 2003). However, there are several possibilities suggested to overcome this problem such as improvements in modeling stellar potentials, subsequent galactic mergers, and gas discs around binaries (see, e.g., Amaro-Seoane et al. 2023), but how this is overcome in nature remains uncertain. These dynamical effects can shrink MBHBs through the sub-parsec regime until GWs become strong enough to drive the binary to merger within a Hubble time. Recently, pulsar timing arrays (EPTA Collaboration et al. 2023; Agazie et al. 2023; Reardon et al. 2023) have provided evidence for a stochastic GW background that is likely sourced by a population of $\geq 10^8 M_\odot$ inspiraling MBHBs, which have made it through the final parsec. If this also occurs for $10^4 - 10^8 M_\odot$ near-equal-mass merging MBHBs, then they will be observable up to redshift $z \sim 20$ by the Laser Interferometer Space Antenna (LISA; Amaro-Seoane et al. 2017; Colpi et al. 2024), recently adopted by ESA.

In the LISA milli-Hz-frequency band, GWs from MBHBs will have high signal-to-noise ratios (SNRs), which will help to constrain source parameters and also put constraints on merging binaries’ environments. The effects of gas are particularly compelling in contrast with those from stellar cluster hardening (Gualandris et al. 2022) because they can leave detectable imprints on the GW waveform

(Barausse et al. 2014; Zwick et al. 2022; Garg et al. 2022; Tiede et al. 2024; Garg et al. 2024a). Prior to merger, gas has also been demonstrated to excite binary eccentricities that may remain measurable in the LISA band (Zrake et al. 2021; Garg et al. 2024b) and gas can also affect the component BH’s spin (Bourne et al. 2023).

For near-equal-mass MBHBs, radiatively efficient gas will settle into a co-planar circumbinary disc (CBD; D’Orazio et al. 2016) with prograde (retrograde) CBDs leading to CBD-aligned mini-discs around each component BH (Farris et al. 2014; Tiede & D’Orazio 2024). While a recent study (Garg et al. 2024a) put constraints on the CBD properties using GWs alone, it also suggests degeneracies between disc parameters that can be broken by electromagnetic (EM) counterparts (Haiman 2017; Mangiagli et al. 2022; D’Orazio & Charisi 2023; Franchini et al. 2024; Cocchiara et al. 2024). Another possibility is to study the population of observed events. Realization of MBHB merger rates at the high end of what is expected for LISA (100’s per year; Amaro-Seoane et al. 2023) would allow us to not only analyze events individually, but also the population and learn underlying properties of source distributions and their environments. This strategy is already employed by ground-based GW detectors to disentangle formation channels for the observed stellar-mass binary BH population (Nishizawa et al. 2016; Breivik et al. 2016; Samsing & D’Orazio 2018; D’Orazio & Samsing 2018; Romero-Shaw et al. 2019, 2020; Zevin et al. 2021; Romero-Shaw et al. 2022).

Recent suites of high-resolution hydrodynamical simulations of CBDs suggest pumping or damping of binary orbital eccentricity depending on binary and disc parameters. In particular, whether the disc settles into a prograde or retrograde configuration can have an important impact on the binary eccentricity evolution, and the rate at which the binary inspirals (if it at all; see, e.g. Muñoz et al. 2019) which could lead to distinguishable parameters in the LISA band

* E-mail: mudit.garg@uzh.ch

for the same starting binary. For prograde accretion scenarios (Zrake et al. 2021; D’Orazio & Duffell 2021; Siwek et al. 2023), gas brings the binary to an equilibrium eccentricity ~ 0.4 , where it shrinks the binary’s semi-major axis until GWs are strong enough to drive the binary to coalescence, re-circularizing the orbit (Peters & Mathews 1963; Peters 1964). In retrograde configurations (Bankert et al. 2015; Schnittman & Krolik 2015; Tiede et al. 2024), there is an eccentricity pumping throughout the evolution until the GWs takeover (but, see also Nixon et al. 2011; Roedig & Sesana 2014 for low-eccentricity behavior). In retrograde discs, the binary also shrinks its semi-major axis at least two-times quicker than in prograde scenarios leading to the possibility of different final masses, spins of the component BHs, and orbital eccentricity near-coalescence for the same starting binary. Here we conduct a quantitative study of the differences between merging MBHBs in the LISA band when driven towards merger via retrograde vs prograde accretion. We show that retrograde configurations yield negative effective spin parameters (χ_{eff} ; Damour 2001) correlated with residual eccentricity near-merger, where both can be readily measured via GW observations. This contrasts with prograde systems and may be unique among all formation channels, offering a possibly distinct indicator of the environmental effects that abetted a binary merger.

2 BINARY EVOLUTION MODEL

Consider the motion of two equal-mass spinning BHs of total redshifted mass M_z at redshift z in a tight eccentric orbit with a detector-frame semi-major axis¹ (SMA) a and eccentricity e embedded in a circumbinary disc (CBD). A prograde (retrograde) CBD implies that the disc’s angular momentum (\vec{L}_{CBD}) is in the same (opposite) direction as the binary’s angular momentum (\vec{L}_{Binary}). Moreover, a prograde (retrograde) CBD leads to CBD-aligned mini-discs around each component BH (D’Orazio & Duffell 2021; Tiede & D’Orazio 2024). We also define a dimensionless spin parameter² $s \equiv cJ/Gm^2 \in (-1, 1)$ for a BH of mass m and a spin angular momentum J with positive (negative) values corresponding to a prograde (retrograde) mini-disc orientation with respect to the BH. Fig. 1 shows a schematic for our system for a retrograde CBD configuration.

s sets the innermost stable circular orbit (ISCO; a_{ISCO}) and radiative efficiency (ϵ) of the accretion onto the BH (Fiacconi et al. 2018):

$$a_{\text{ISCO}} = F(s)Gm/c^2, \quad \epsilon = 1 - \sqrt{1 - 2/3F}, \quad (1)$$

$$F(s) = 3 + Z_2 \mp \sqrt{(3 - Z_1)(3 + Z_1 + 2Z_2)},$$

$$Z_1 = 1 + (1 - s^2)^{\frac{1}{3}} [(1 + s)^{\frac{1}{3}} + (1 - s)^{\frac{1}{3}}], \quad Z_2 = \sqrt{3s^2 + Z_1^2},$$

where upper (lower) sign represents a prograde (retrograde) mini-disc configuration.

The evolution of a spin (s_i) that is fully (anti-) aligned with its co-planar mini-disc (*i.e.*, $\theta_i = 0$) is (Fiacconi et al. 2018)

$$\dot{s}_i = \frac{\dot{M}_{z,i}}{M_{z,i}} \left(\frac{F^2 \mp 2s_i\sqrt{F} + s_i^2}{F\sqrt{F - 3 \pm 2s_i/\sqrt{F}}} \frac{1}{1 - \epsilon_i} - 2s_i \right) = \frac{\dot{M}_{z,i}}{M_{z,i}} \tilde{F}(s_i), \quad (2)$$

where again upper (lower) sign represents a prograde (retrograde) mini-disc orientation and $M_{z,i} = M_z/2$. Here $M_{z,i}$ is the accretion

¹ Detector-frame SMA is $(1 + z)$ times the source-frame SMA, since redshifted orbital frequency $\propto \sqrt{M_z/a^3}$.

² Here G is the gravitational constant and c is the speed of light.

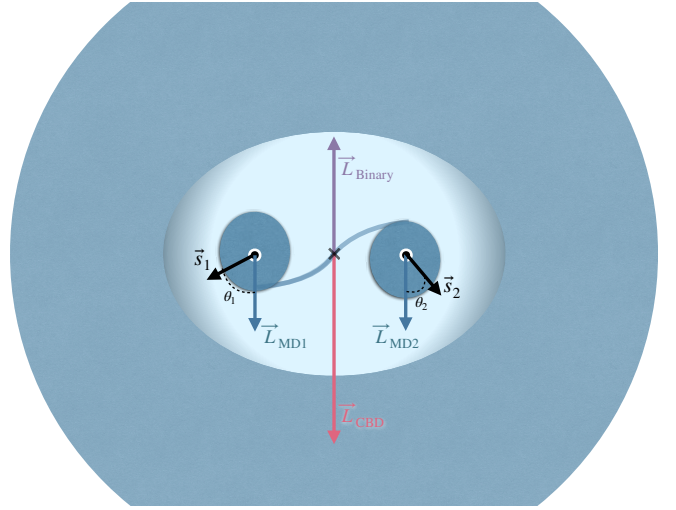


Figure 1. Schematic for a retrograde CBD configuration, where the binary with angular momentum \vec{L}_{Binary} is anti-aligned with that of the accretion disc \vec{L}_{CBD} . The two component BHs have spin vectors $\vec{s}_{1,2}$, which are misaligned by an angle $\theta_{1,2} \in [0, \pi/2)$ with respect to their own CBD-aligned mini-discs of angular momenta $\vec{L}_{\text{MD}1,2}$.

rate onto the component BH and determined by the steady-state accretion rate at infinity $\dot{M}_0 \equiv \dot{f}_{\text{Edd}} M_z / 45 \text{ Myr}^{-1}$ (Jiang et al. 2014) via $\dot{M}_{z,i} = (1 - \epsilon_i) \dot{M}_0 / 2$. Assuming \dot{M}_0 is split evenly between both component BHs, motivated by measured preferential accretion for both prograde and retrograde CBDs (D’Orazio et al. 2024), we can write down the accretion rate onto the binary

$$\dot{M}_z = \left(1 - \frac{\epsilon_1 + \epsilon_2}{2}\right) \dot{M}_0 = \left(1 - \frac{\epsilon_1 + \epsilon_2}{2}\right) \frac{\dot{f}_{\text{Edd}}}{45 \text{ Myr}} M_z, \quad (3)$$

where \dot{f}_{Edd} is the Eddington ratio and ϵ_i is the efficiency of the i -th component BH. We assume \dot{M}_0 or equivalently \dot{f}_{Edd} are constant throughout the binary evolution, *i.e.*, the feeding rate to the disc at infinity is constant.

For an equal-mass MBHB embedded in a co-planar circumbinary disc (CBD), the details of the accretion flow and binary-disc parameters dictate if the gas torques the binary to inspiral or outspiral. For a retrograde disc, the evolution of SMA and eccentricity due to gas are (Tiede & D’Orazio 2024)

$$\dot{a}_{\text{gas}}^{\text{ret}} \approx -10 \frac{\dot{M}_z}{M_z} a, \quad \dot{e}_{\text{gas}}^{\text{ret}} \approx \frac{\dot{M}_z}{M_z} \begin{cases} 20e, & e \leq 0.15, \\ 3, & e > 0.15. \end{cases} \quad (4)$$

While for the prograde binary, we take $\dot{e}_{\text{gas}}^{\text{pro}}$ from the Zrake et al. (2021) fit and the most negative value of $\dot{a}_{\text{gas}}^{\text{pro}}$ from D’Orazio & Duffell (2021) to consider the fastest merger timescale:

$$\dot{a}_{\text{gas}}^{\text{pro}} = -5 \frac{\dot{M}_z}{M_z} a. \quad (5)$$

We also always initialize prograde binaries from their equilibrium eccentricity $e_{\text{eq}}^{\text{pro}} = 0.45$ (Zrake et al. 2021; D’Orazio & Duffell 2021; Siwek et al. 2023), where binaries only circularize when GW emission becomes dominant over gas effects. This will result in the fastest inspiral times for the prograde case to compare with retrograde results computed later. Slower inspiral times will only exacerbate the differences we later find between the two disc configurations.

GWs remove energy and angular momentum from a compact MBHB. At Newtonian-order, orbit-averaged evolution rates for a and e due to emission of GWs are (Peters & Mathews 1963; Peters

1964)

$$\dot{a}_{\text{GW}} = -\frac{16}{5} \frac{G^3}{c^5} \frac{M_z^3}{a^3} \left(1 + \frac{73}{24} e^2 + \frac{37}{96} e^4 \right) (1 - e^2)^{-\frac{7}{2}}, \quad (6)$$

$$\dot{e}_{\text{GW}} = -e \frac{76}{15} \frac{G^3}{c^5} \frac{M_z^3}{a^4} \left(1 + \frac{121}{304} e^2 \right) (1 - e^2)^{-\frac{5}{2}}.$$

Even though retrograde configurations in § 3 will induce high eccentricities during binary evolution, we have checked that we never reach the relativistic regime to require higher post-Newtonian terms.

We choose to begin our binary evolution from the self-gravitating radius (R_{sg}) of a thin CBD. Beyond this, the disc can fragment, or calculations including disc self-gravity are required (see, e.g. [Franchini et al. 2021](#)). Furthermore, we argue that this is the valid limit for the $M_z \lesssim 10^7$ MBHBs in the LISA band. For a turbulo-viscous parameter $\alpha = 0.1$ ([Shakura & Sunyaev 1973](#)), the self-gravitating radius can be expressed as ([Bortolas et al. 2021](#))

$$R_{\text{sg}}[r_s] = 5.32 \times 10^6 (f_{\text{Edd}}/0.1)^{-\frac{22}{45}} \left(M_z/10^5 M_\odot \right)^{-\frac{52}{45}}, \quad (7)$$

where $r_s \equiv 2GM_z/c^2$ is the Schwarzschild radius of the total binary mass. For MBHBs in the LISA band, R_{sg} is much larger than the separation scale where GW inspiral will outpace the CBD and gas effects are no longer important ($a \lesssim 10^2 R_{\text{sg}}$; see, e.g. [Dittmann et al. 2023](#)). Hence, for the lower-mass LISA MBHBs, we are justified in using Eqs (4) and (5), as a gravitationally stable CBD will surround such MBHBs during a long duration of inspiral where gas effects can dominate over GW-driven evolution. Therefore, we consider earlier evolution of the MBHB via stars or gravitationally unstable gas as setting our initial conditions, which will primarily dictate final values of binary parameters in § 3.

We assume that the binary is always fully (anti-) aligned with its CBD at least by the time the system is initialized at the self-gravitating radius. For mild initial misalignment, it takes around a few Myr for complete (anti-) alignment ([Martin & Lubow 2019](#)). Moreover, we assume that the magnitude and misalignment angle of the component BH's spin vector evolve independently from each other. We also always assume that the BH spins (anti-) align with their mini-discs when the binary reaches the LISA band. The spin-alignment timescale is at maximum ~ 60 Myr for an already maximally spinning BH with almost $\pi/2$ radians misalignment for $f_{\text{Edd}} = 0.1$ and azimuthal Mach number 10. Therefore, for almost all parameters considered, the BH spins will fully align with their mini-discs, and only for a narrow set of parameters will some residual misalignment remain near merger. This can be seen later in Fig. 2, where only for initial eccentricities $e_0 \gtrsim 0.6$, inspiral timescales are less than 60 Myr. Our spin-alignment assumption is further supported by [Bourne et al. \(2023\)](#), where they almost always find spin alignment irrespective of the disc orientation and initial eccentricity.

To study the evolution of binary parameters under the influence of both GWs and CBD, we evolve the following coupled equations from $a = R_{\text{sg}}$ to 1 year before merger³ in the LISA band:

$$\dot{a} = \dot{a}_{\text{GW}} + \dot{a}_{\text{gas}}, \quad \dot{e} = \dot{e}_{\text{GW}} + \dot{e}_{\text{gas}}, \quad (8)$$

$$\frac{\dot{M}_z}{M_z} = \left(1 - \frac{\epsilon_1 + \epsilon_2}{2} \right) \frac{f_{\text{Edd}}}{45 \text{ Myr}}, \quad \dot{s}_1 = \frac{\dot{M}_{z,1}}{M_{z,1}} \tilde{F}(s_1), \quad \& \quad \dot{s}_2 = \frac{\dot{M}_{z,2}}{M_{z,2}} \tilde{F}(s_2),$$

where \dot{a}_{gas} is $\dot{a}_{\text{gas}}^{\text{pro}}$ ($\dot{a}_{\text{gas}}^{\text{ret}}$) for the prograde (retrograde) CBD.

In the next section, we evolve our systems of interest under the

e_0	$t_{\text{ins}} [\text{Myr}]$	$e_{1\text{yr}}$	$M_z/M_{z,0}$	$s_{1,2}$
0	370	0	2.03	0.99
0.1	149	0.03	1.35	0.73
0.2	130	0.05	1.31	0.67
0.3	113	0.06	1.26	0.62
0.4	97	0.09	1.22	0.55
0.5	81	0.12	1.18	0.48
0.6	64	0.16	1.14	0.41
0.7	48	0.21	1.11	0.32
0.8	32	0.27	1.07	0.22

Table 1. The initial eccentricity (e_0), the inspiral timescale (t_{ins}), the eccentricity one year before merger ($e_{1\text{yr}}$), the final-to-initial total mass ratio, and final spins assuming $f_{\text{Edd}} = 0.1$, initial total mass $M_{z,0} = 10^5 M_\odot$, and zero initial spins, for retrograde evolution.

influence of both gas and GWs to find expected binary parameters in the LISA band.

3 RESULTS

3.1 Relevant timescales

We solve the coupled equations in Eq. (8) for the retrograde system for $f_{\text{Edd}} = 0.1$, $z = 1$, an initial total mass $M_{z,0} = 10^5 M_\odot$, initial spins $s_{1,2} = 0$, and for various initial eccentricities e_0 . In Table 1, we show the corresponding inspiral timescale t_{ins} , eccentricity one-year before merger ($e_{1\text{yr}}$), the final-to-initial total-mass ratio, and final spins. Here, $M_z/M_{z,0}$ can be well approximated by $\exp(f_{\text{Edd}} t_{\text{ins}}/50 \text{ Myr})$. We can infer from $s_{1,2} > 0$ that retrograde accretion leads to component BH spins aligned with their mini-discs and anti-aligned with the binary. Increasing the total mass to $M_{z,0} = 10^6 M_\odot$ does not meaningfully alter t_{ins} for retrograde binaries,⁴ but $e_{1\text{yr}}$ decreases by a factor of 5 from the $M = 10^5 M_\odot$ case for a given e_0 . While for a prograde binary, $e_{1\text{yr}} \sim 10^{-3}$, irrespective of the initial total mass. Increasing the accretion rate to $f_{\text{Edd}} = 1$ results in a nearly ten times faster inspiral time as well as slightly higher eccentricities for retrograde CBDs and $e_{1\text{yr}} \sim 10^{-2.5}$ for prograde scenarios. While the final spins are almost independent of f_{Edd} , we further discuss spin evolution in § 3.2.

In Fig. 2, as a function of e_0 , we compare spin-up timescales from different initial spin magnitudes, binary lifetimes for different configurations, and a typical CBD lifetime based on observations of AGN. We see that the prograde systems live longer than their spin-up timescales for any s_0 , while retrograde systems have lifespans shorter than the spin-up timescale. This implies that prograde systems will always maximally spin up their component BHs to align with the orbital angular momentum while in retrograde scenarios this happens only for initially highly spinning component BHs aligned with their minidisks (and so anti-aligned with the binary, i.e., $s_0 \sim 1$). We further explore retrograde spin-up in the next sub-section.

The observationally motivated CBD lifetime for $f_{\text{Edd}} \gtrsim 0.1$ is around 100 Myr ([Hopkins & Hernquist 2009](#)), for masses relevant to LISA. This implies that for $f_{\text{Edd}} = 0.1$, MBHBs initialized from the self-gravitating radius with either prograde CBDs or retrograde

³ SMA, one year before merging, is calculated by integrating \dot{a}_{GW} with final separation a_{ISCO} .

⁴ Except for $e_0 = 0$ case, where $t_{\text{ins}} \sim 250 \text{ Myr}$.

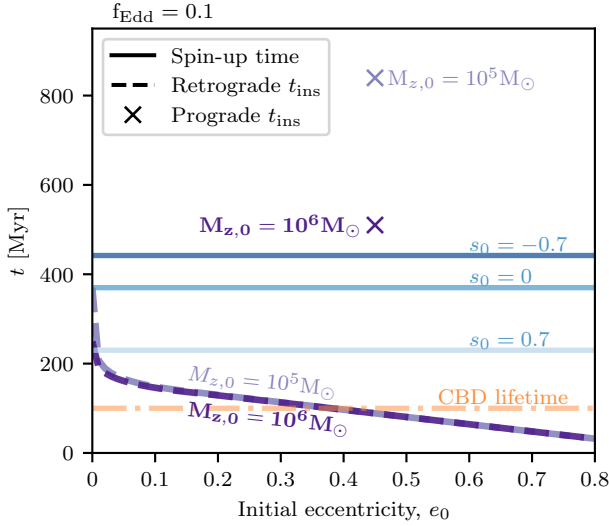


Figure 2. Timescales of interest for $f_{\text{Edd}} = 0.1$ as a function of initial eccentricity e_0 . We show inspiral timescales (dashed lines) for two initial total masses $M_{z,0} = 10^5 M_\odot$ (light purple) and $M_{z,0} = 10^6 M_\odot$ (dark purple) in a retrograde CBD starting from the self-gravitating radius of the disc. For comparison, we show prograde results (x’s) for the same masses initialized at $e_0 = 0.45$. We also show spin-up timescales (solid lines) for a component BH to increase its spin to $s_i = 0.99$ from three initial spins. We draw an expected, 100 Myr, CBD lifetime as the dot-dashed orange line.

CBDs with low initial binary eccentricity ($e_0 \lesssim 0.3$) will not reach the LISA band. To consider this, § 3.3 shows population results for three scenarios: no restriction on inspiral timescale, $t_{\text{ins}} \lesssim 100$ Myr restriction by starting longer inspiral systems closer than R_{sg} , and only considering R_{sg} initialized MBHBs that merge within the CBD lifetime, *i.e.*, $t_{\text{ins}}^{\text{sg}} < 100$ Myr.

3.2 Spin evolution

Despite retrograde binary lifetimes being shorter than the typical spin-up time, a significant imprint on the effective spin in the LISA band can still arise for retrograde systems.

The effective spin of the binary χ_{eff} assuming complete (anti-) alignment is (Damour 2001)

$$\chi_{\text{eff}} = \frac{s_1 + s_2}{2} \times \begin{cases} +1, & \text{for prograde CBD,} \\ -1, & \text{for retrograde CBD.} \end{cases} \quad (9)$$

Fig. 3 plots the expected effective spin one-year before merger ($\chi_{\text{eff},1\text{yr}}$) for retrograde evolution for a few systems of interests. Low initial eccentricities lead to longer inspiral timescales (see Fig. 2), allowing more time for the mini-discs to spin-up the BHs, resulting in more negative $\chi_{\text{eff},1\text{yr}}$ for retrograde binaries.

3.3 Population

We are interested in estimating the expected distribution for the effective spin ($\chi_{\text{eff},1\text{yr}}$) and the eccentricity ($e_{1\text{yr}}$), one-year before merger, when LISA can probe it. To do so we realize a population by drawing the parameters described in Sec. 2 as follows:

- For initial total masses, we relate $M_{z,0}$ to the MBHB’s luminosity $L = f_{\text{Edd}} L_{\text{Edd}}$, where the Eddington luminosity $L_{\text{Edd}} \equiv 6.3 \times 10^4 M_{z,0} \text{ ergs s}^{-1}$ and then draw L from the observed

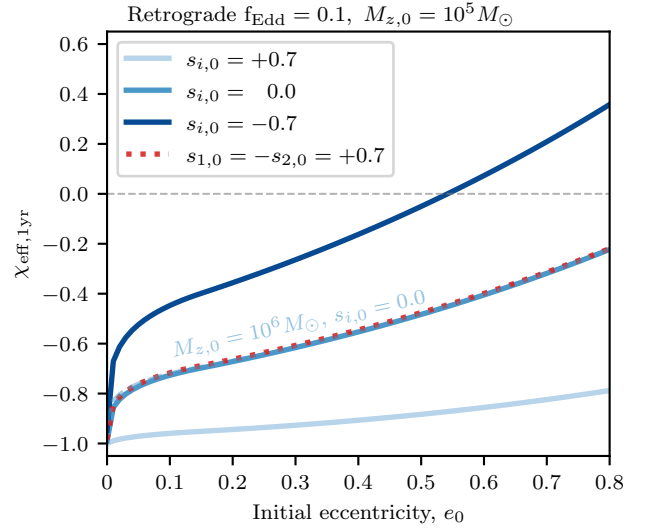


Figure 3. Effective spin $\chi_{\text{eff},1\text{yr}}$, one year before merger for a $M_{z,0} = 10^5 M_\odot$ (solid line) MBHB with $f_{\text{Edd}} = 0.1$ retrograde CBD, as a function of the initial eccentricity e_0 for different initial spin configurations. We also include $M_{z,0} = 10^6 M_\odot$ (dashed medium blue) with zero initial spins for comparison.

quasar luminosity function (QLF) at redshift $z = 1$ and $z = 2$ (Hopkins et al. 2007), where expected merger rate for gas-embedded MBHBs is highest (see, *e.g.* Salcido et al. 2016). Moreover, to have events in the LISA band, we only consider initial total masses $M_{z,0} \sim [10^{4.5}, 10^7] M_\odot$ for retrograde MBHBs and $M_{z,0} \sim [10^4, 10^7] M_\odot$ for prograde MBHBs. Different initial mass ranges are needed to get the same distribution of total masses $\sim [10^{4.5}, 10^{7.5}] M_\odot$ in the LISA band since the prograde inspiral timescale is much larger than in the retrograde case leading to larger increases in mass.

- We draw initial spin magnitudes and eccentricities from uniform distributions: $s_0 \sim \text{Uniform}(-1, 1)$ and $e_0 \sim \text{Uniform}(0, 0.8)$.

We initialized 100 MBHBs from their CBD’s self-gravitating radius, such that all events have SNR of at least 8 at $z = 1$ in the LISA band to be observable (Garg et al. 2022) and to mimic expected MBHB detections by LISA (Amaro-Seoane et al. 2023). For both retrograde and prograde MBHBs, we show $\chi_{\text{eff},1\text{yr}}$ vs $e_{1\text{yr}}$ in Fig. 4 at redshift $z = 1$ and $f_{\text{Edd}} = 0.1$. We find that prograde CBDs lead to almost positive unity effective spin and non-measurable $e_{1\text{yr}}$, and in the retrograde case, we mostly have negative $\chi_{\text{eff},1\text{yr}}$ and measurable eccentricities.⁵

Assuming all binaries are brought to merger by an accretion phase, Fig. 4 shows that one could distinguish between prograde and retrograde from their $\chi_{\text{eff},1\text{yr}}$ vs $e_{1\text{yr}}$ correlations in the LISA band, as they occupy different parts of the parameter space. Note that, even for the fastest inspiral case in prograde, we predict almost unity effective spin such that this should also be the case for more complex evolutions $a_{\text{gas}}^{\text{pro}}$ (see, *e.g.* D’Orazio & Duffell 2021). Similarly, $e_{1\text{yr}}$ for prograde scenarios should be the same for equal-mass MBHBs (Zrake et al. 2021) as it is only a function of the equilibrium value $e_{\text{eq}}^{\text{pro}} = 0.45$ (see also Siwek et al. 2023; Valli et al. 2024). Thus we expect that our prograde results are robust despite the simplifications.

In Fig. 5, we repeat this experiment for 10^4 LISA-observable events

⁵ An equal-mass merging MBHB with $M_z = 10^5 M_\odot$ has the minimum measurable eccentricity $10^{-2.75}$ at $z = 1$ for a one-year observation window (Garg et al. 2024a).

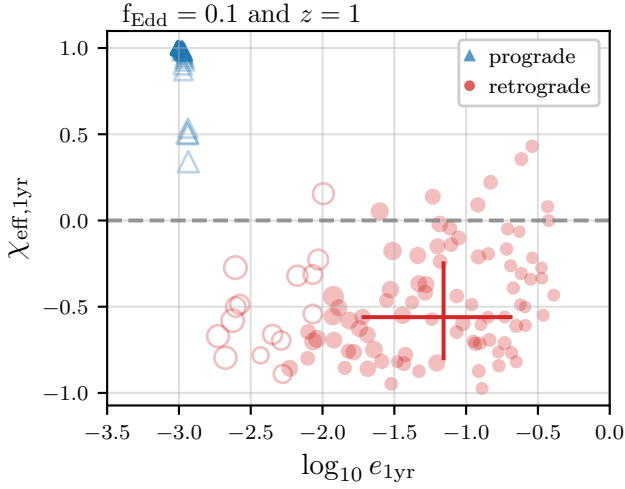


Figure 4. $\chi_{\text{eff},1\text{yr}}$ vs $e_{1\text{yr}}$ for 100 LISA-observable MBHBs at $z = 1$ for prograde (blue triangles) and retrograde (red circles) CBDs with $f_{\text{Edd}} = 0.1$ Eddington ratio. The marker size represents how large M_z is in the range $\sim [10^{4.5}, 10^{7.5}] M_\odot$. Filled symbols corresponds to measurable eccentricity ($e_{1\text{yr}}^{\text{det}}$) as per Garg et al. (2024b,a). For retrograde systems, we draw solid red bars indicating 68 per cent credible intervals of spin-eccentricity distribution with intersection indicating median values.

Scenario	$\log_{10} e_{1\text{yr}}^{\text{det}}$	$\chi_{\text{eff},1\text{yr}}$
Fiducial	$-1.16^{+0.48}_{-0.57}$	$-0.56^{+0.32}_{-0.25}$
$f_{\text{Edd}} = 1$	$-1.03^{+0.48}_{-0.57}$	$-0.57^{+0.32}_{-0.24}$
$z = 2$	$-1.16^{+0.48}_{-0.56}$	$-0.56^{+0.33}_{-0.24}$
$t_{\text{ins}} < 100 \text{ Myr}$	$-0.96^{+0.40}_{-0.76}$	$-0.43^{+0.30}_{-0.27}$
$t_{\text{ins}}^{\text{sg}} < 100 \text{ Myr}$	$-0.90^{+0.34}_{-0.58}$	$-0.40^{+0.31}_{-0.27}$
$e_{\text{eq}}^{\text{ret}} = 0.9$	$-2.38^{+0.01}_{-0.02}$	$-0.95^{+0.06}_{-0.04}$
$e_{\text{eq}}^{\text{ret}} = 0.99$	$-1.79^{+0.01}_{-0.03}$	$-0.75^{+0.23}_{-0.15}$
$e_{\text{eq}}^{\text{ret}} = 0.999$	$-1.21^{+0.02}_{-0.50}$	$-0.58^{+0.29}_{-0.23}$

Table 2. Measurable eccentricity ($e_{1\text{yr}}^{\text{det}}$) and effective spin distributions for different scenarios in Fig. 5.

for varying scenarios to better ascertain the underlying distributions and minimize variance from drawing fewer events. In comparison to our fiducial retrograde case with Eddington ratio $f_{\text{Edd}} = 0.1$ and redshift $z = 1$, we consider $f_{\text{Edd}} = 1$, $z = 2$, and CBD-lifetime restricted inspirals: either $t_{\text{ins}} < 100 \text{ Myr}$ or only considering events which merge with $t_{\text{ins}}^{\text{sg}} < 100 \text{ Myr}$, when initialized from the self-gravity radius. We also consider different maximum equilibrium eccentricities (dubbed $e_{\text{eq}}^{\text{ret}}$) for the retrograde CBD. That is to say, one might imagine that retrograde discs can only pump eccentricity to some maximum value $e_{\text{eq}}^{\text{ret}}$ at which shock-dissipation at pericenter (or some other mechanism) could shut off eccentricity growth. In such a scenario, the MBHB will stall at $e_{\text{eq}}^{\text{ret}}$, keep shrinking due to $\dot{a}_{\text{gas}}^{\text{ret}}$, and will circularize when GWs become dominant. Lowering $e_{\text{eq}}^{\text{ret}}$ results in longer inspiral timescales and more negative $\chi_{\text{eff},1\text{yr}}$, but smaller $e_{1\text{yr}}^{\text{det}}$. We note, however, that each of these scenarios in Fig. 5 retains an in-band eccentricity above the $e_{1\text{yr}} > 10^{-2.75}$ detection threshold for an equal-mass $10^5 M_\odot$ binary.

Both redshifts produce similar spin-eccentricity correlations, implying that our results are independent of redshift. This is because

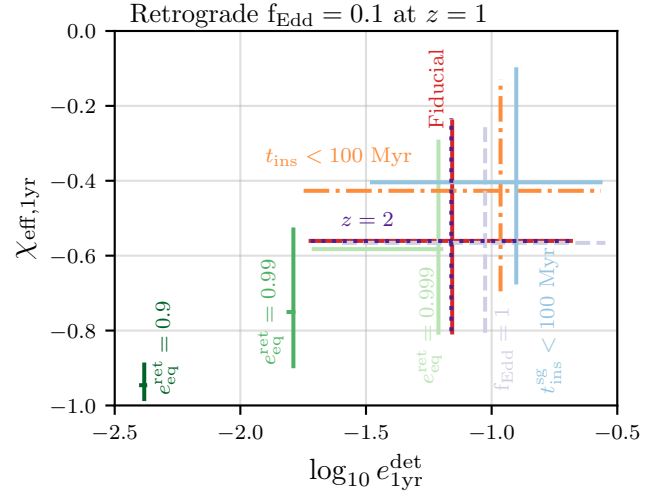


Figure 5. Spin-eccentricity correlations for MBHBs with detectable eccentricity ($e_{1\text{yr}}^{\text{det}}$) for different scenarios in comparison to our fiducial retrograde CBD (solid red) with $f_{\text{Edd}} = 0.1$ at $z = 1$. We show $f_{\text{Edd}} = 1$ (dashed light purple), $z = 2$ (dotted dark purple), $t_{\text{ins}} < 100 \text{ Myr}$ (dot-dashed orange), $t_{\text{ins}}^{\text{sg}} < 100 \text{ Myr}$ (solid medium blue), and assuming the maximum eccentricity in retrograde ($e_{\text{eq}}^{\text{ret}}$) to be either 0.9 (solid dark green), 0.99 (solid medium green), and 0.999 (solid light green). Bars are similar to Fig. 4 and we summarize these bounds in Table 2.

once we consider detector-frame quantities, a fixed range for total masses $M_z \sim [10^{4.5}, 10^{7.5}] M_\odot$, and the same number of observable events, then only QLF, SNR, and the minimum measurable eccentricity changes with redshift. QLF's shape depends weakly on z , SNRs are still higher than our threshold of 8 at $z = 2$, and the minimum measurable eccentricity only increases slightly at $z = 2$, effectively, not changing results at different redshifts. While spin distributions are almost the same for both Eddington ratios $f_{\text{Edd}} = 0.1$ and $f_{\text{Edd}} = 1$, $e_{1\text{yr}}^{\text{det}}$ is slightly higher for the latter and this could help to distinguish between Eddington ratios.⁶ Limiting the inspiral timescale to typical AGN lifetimes of 100 Myr leads to higher effective spin and higher measurable eccentricities. The former is because smaller initial eccentricities are time limited and not able to spin BHs to high negative effective spin as per Figs 2 and 3 and the latter because higher initial eccentricities are selected because they merge more quickly.

4 DISCUSSION AND CONCLUSION

We find that MBHBs with a retrograde CBD typically have negative $\chi_{\text{eff},1\text{yr}}$ and measurable eccentricity in the LISA band in comparison to prograde scenarios, which results in positive effective spin and usually non-measurable $e_{1\text{yr}}$. Moreover, the spin-eccentricity distribution of binaries evolving through a retrograde accretion channel occupy a unique part of parameter space that appears to be robust to environmental or evolutionary parameters such as f_{Edd} , redshift, or $e_{\text{eq}}^{\text{ret}}$. However, different parameters could change the exact quantitative spin-eccentricity correlations, which may update with advances in simulating CBD-driven orbital evolution.

An observation of even a single negative effective spin event with

⁶ For prograde case, $f_{\text{Edd}} = 1$ still has unity $\chi_{\text{eff},1\text{yr}}$ but $e_{1\text{yr}} \sim 10^{-2.5}$ instead of $e_{1\text{yr}} \sim 10^{-3}$ for 0.1 Eddington ratio.

detectable eccentricity combined with a measurement of a GW’s phase perturbation at the -4 post-Newtonian order (Garg et al. 2024a) could provide a strong hint towards a retrograde CBD. The latter can help to distinguish over other channels (Zwick et al. 2023), such as hardening due to a third MBH (Bonetti et al. 2019) or chaotic accretion (King & Pringle 2006). Additionally, if we detect an EM counterpart for an MBHB that confirms the presence of an accretion disc (see, e.g. Mangiagli et al. 2022), then a positive (negative) effective spin can provide evidence towards prograde/retrograde CBD orientations, even for a non-measurable eccentricity. The full population of observations may also yield insights on the relative importance of disc-mediated phases in massive binary evolution.

We have relied on a number of assumptions that might be relaxed in the future: While the hydrodynamical simulation results in Tiede & D’Orazio (2024) are only computed for eccentricity up to 0.8, we extrapolate them to higher eccentricities. Furthermore, existing hydrodynamical results that span a sufficient range of orbital eccentricities derive from 2D, isothermal hydrodynamical treatments of the CBD. While the key ingredients of retrograde eccentricity pumping (for, e.g., 3D, self-gravitating disks, including magnetic fields, or unequal masses Nixon et al. 2011; Roedig & Sesana 2014; Bankert et al. 2015; Amaro-Seoane et al. 2016) and retrograde mini-disks (Tiede & D’Orazio 2024) appear to be robust, inclusion of more complete physics in future simulations will be necessary to improve the accuracy of the predictions presented here. Moreover, we add evolution rates from gas and GWs linearly as it is not possible to infer cross terms from current simulations for MBHBs. However, studies by Derdzinski et al. (2019, 2021) suggest that for extreme mass ratio inspirals cross terms should be weak, which may also extend to MBHBs. Peters (1964) results for the binary evolution under GW emission may also breakdown for extremely high eccentricities due to errors in the orbital averaging not capturing the correct rates (Fumagalli & Gerosa 2023). However, this is not clear how it will affect our results and we leave this for future work. We additionally only consider equal-mass MBHBs, due to the limitation of retrograde results and under the assumption that before reaching the self-gravitating radius the binary has become close to equal-mass through preferential accretion.

In summary, we have demonstrated a possibly unique signature of the retrograde CBD accretion channel comprising MBHB mergers with negative effective spin and measurable eccentricities that will help to distinguish from other binary formation scenarios such as prograde accretion, stellar hardening, and third-body interactions.

DATA AVAILABILITY STATEMENT

The data underlying this article will be shared on reasonable request to the authors.

ACKNOWLEDGEMENTS

MG acknowledge support from the Swiss National Science Foundation (SNSF) under the grant 200020_192092. D.J.D. and C.T. received support from the Danish Independent Research Fund through Sapere Aude Starting grant No. 121587. The authors also acknowledge use of the NumPy (Harris et al. 2020) and Matplotlib (Hunter 2007).

REFERENCES

- Agazie G., et al., 2023, *ApJ*, **951**, L8
- Amaro-Seoane P., Maureira-Fredes C., Dotti M., Colpi M., 2016, arXiv.org, p. arXiv:1604.01392
- Amaro-Seoane P., et al., 2017, arXiv e-prints, p. arXiv:1702.00786
- Amaro-Seoane P., et al., 2023, *Living Reviews in Relativity*, **26**, 2
- Bankert J., Krolik J. H., Shi J., 2015, *The Astrophysical Journal*, **801**, 114
- Barausse E., Cardoso V., Pani P., 2014, *Phys. Rev. D*, **89**, 104059
- Begelman M. C., Blandford R. D., Rees M. J., 1980, *Nature*, **287**, 307
- Bonetti M., Sesana A., Haardt F., Barausse E., Colpi M., 2019, *MNRAS*, **486**, 4044
- Bortolas E., Franchini A., Bonetti M., Sesana A., 2021, *ApJ*, **918**, L15
- Bourne M. A., Fiacconi D., Sijacki D., Piotrowska J. M., Koudmani S., 2023, arXiv e-prints, p. arXiv:2311.17144
- Breivik K., Rodriguez C. L., Larson S. L., Kalogera V., Rasio F. A., 2016, *ApJ*, **830**, L18
- Cocchiararo F., Franchini A., Lupi A., Sesana A., 2024, arXiv e-prints, p. arXiv:2402.05175
- Colpi M., et al., 2024, arXiv e-prints, p. arXiv:2402.07571
- D’Orazio D. J., Charisi M., 2023, arXiv e-prints, p. arXiv:2310.16896
- D’Orazio D. J., Duffell P. C., 2021, *ApJ*, **914**, L21
- D’Orazio D. J., Samsing J., 2018, *MNRAS*, **481**, 4775
- D’Orazio D. J., Haiman Z., Duffell P., MacFadyen A. I., Farris B. D., 2016, *Mon. Not. Roy. Astron. Soc.*, **459**, 2379
- D’Orazio D. J., Duffell P. C., Tiede C., 2024, arXiv e-prints, p. arXiv:2403.05629
- Damour T., 2001, *Phys. Rev. D*, **64**, 124013
- Derdzinski A. M., D’Orazio D., Duffell P., Haiman Z., MacFadyen A., 2019, *MNRAS*, **486**, 2754
- Derdzinski A., D’Orazio D., Duffell P., Haiman Z., MacFadyen A., 2021, *MNRAS*, **501**, 3540
- Dittmann A. J., Ryan G., Miller M. C., 2023, *ApJ*, **949**, L30
- EPTA Collaboration et al., 2023, *A&A*, **678**, A50
- Farris B. D., Duffell P., MacFadyen A. I., Haiman Z., 2014, *ApJ*, **783**, 134
- Fiacconi D., Sijacki D., Pringle J. E., 2018, *MNRAS*, **477**, 3807
- Franchini A., Sesana A., Dotti M., 2021, *MNRAS*, **507**, 1458
- Franchini A., Bonetti M., Lupi A., Sesana A., 2024, arXiv e-prints, p. arXiv:2401.10331
- Fumagalli G., Gerosa D., 2023, *Phys. Rev. D*, **108**, 124055
- Garg M., Derdzinski A., Zwick L., Capelo P. R., Mayer L., 2022, *MNRAS*, **517**, 1339
- Garg M., Derdzinski A., Tiwari S., Gair J., Mayer L., 2024a, arXiv e-prints, p. arXiv:2402.14058
- Garg M., Tiwari S., Derdzinski A., Baker J. G., Marsat S., Mayer L., 2024b, *MNRAS*, **528**, 4176
- Gualandris A., Khan F. M., Bortolas E., Bonetti M., Sesana A., Berczik P., Holley-Bockelmann K., 2022, *MNRAS*, **511**, 4753
- Haiman Z., 2017, *Phys. Rev. D*, **96**, 023004
- Harris C. R., et al., 2020, *Nature*, **585**, 357
- Hopkins P. F., Hernquist L., 2009, *ApJ*, **698**, 1550
- Hopkins P. F., Richards G. T., Hernquist L., 2007, *ApJ*, **654**, 731
- Hunter J. D., 2007, *Computing in Science & Engineering*, **9**, 90
- Jiang Y.-F., Stone J. M., Davis S. W., 2014, *ApJ*, **796**, 106
- King A. R., Pringle J. E., 2006, *MNRAS*, **373**, L90
- Mangiagli A., Caprini C., Volonteri M., Marsat S., Vergani S., Tamanini N., Inchauspé H., 2022, *Phys. Rev. D*, **106**, 103017
- Martin R. G., Lubow S. H., 2019, *MNRAS*, **490**, 1332
- Milosavljevic M., Merritt D., 2003, *AIP Conf. Proc.*, **686**, 201
- Muñoz D. J., Miranda R., Lai D., 2019, *ApJ*, **871**, 84
- Nishizawa A., Berti E., Klein A., Sesana A., 2016, *Phys. Rev. D*, **94**, 064020
- Nixon C. J., Cossins P. J., King A. R., Pringle J. E., 2011, *MNRAS*, **412**, 1591
- Peters P. C., 1964, PhD thesis, California Institute of Technology
- Peters P. C., Mathews J., 1963, *Physical Review*, **131**, 435
- Reardon D. J., et al., 2023, *ApJ*, **951**, L6
- Roedig C., Sesana A., 2014, *MNRAS*, **439**, 3476
- Romero-Shaw I. M., Lasky P. D., Thrane E., 2019, *MNRAS*, **490**, 5210

- Romero-Shaw I., Lasky P. D., Thrane E., Calderón Bustillo J., 2020, [ApJ](#), **903**, L5
- Romero-Shaw I., Lasky P. D., Thrane E., 2022, [ApJ](#), **940**, 171
- Salcido J., Bower R. G., Theuns T., McAlpine S., Schaller M., Crain R. A., Schaye J., Regan J., 2016, [MNRAS](#), **463**, 870
- Samsing J., D’Orazio D. J., 2018, [MNRAS](#), **481**, 5445
- Schnittman J. D., Krolik J. H., 2015, [ApJ](#), **806**, 88
- Shakura N. I., Sunyaev R. A., 1973, [A&A](#), **500**, 33
- Siwek M., Weinberger R., Hernquist L., 2023, [MNRAS](#), **522**, 2707
- Tiede C., D’Orazio D. J., 2024, [MNRAS](#), **527**, 6021
- Tiede C., D’Orazio D. J., Zwick L., Duffell P. C., 2024, [ApJ](#), **964**, 46
- Valli R., et al., 2024, [arXiv e-prints](#), p. [arXiv:2401.17355](#)
- Zevin M., Romero-Shaw I. M., Kremer K., Thrane E., Lasky P. D., 2021, [ApJ](#), **921**, L43
- Zrake J., Tiede C., MacFadyen A., Haiman Z., 2021, [ApJ](#), **909**, L13
- Zwick L., Derdzinski A., Garg M., Capelo P. R., Mayer L., 2022, [MNRAS](#), **511**, 6143
- Zwick L., Capelo P. R., Mayer L., 2023, [MNRAS](#), **521**, 4645

This paper has been typeset from a \LaTeX file prepared by the author.